Available online at www.sciencedirect.com

ScienceDirect

journal homepage: www.elsevier.com/locate/he

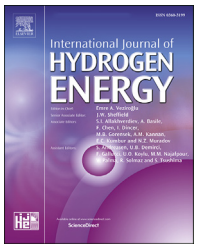

Turbulent flame structure characteristics of hydrogen enriched natural gas with CO_2 dilution

Meng Zhang, Jinhua Wang, Zuohua Huang*

State Key Laboratory of Multiphase Flow in Power Engineering, Xi'an Jiaotong University, Xi'an, 710049, China

HIGHLIGHTS

- The H_2 enrichment turbulent flames diluted with CO_2 were measured by PLIF.
- H_2 addition results larger S_T/S_L while CO_2 dilution decreases S_T/S_L.
- The local curvature radius is a better parameter to indicate the flame front scales.
- H_2/CO_2 addition can be a potential method for adjusting the combustion intensity.

ARTICLE INFO

Article history:
Received 8 August 2019
Received in revised form
7 November 2019
Accepted 5 December 2019
Available online 28 December 2019

Keywords:
Turbulent premixed flame
Hydrogen addition
CO_2 dilution
Flame front structure
Flame curvature

ABSTRACT

This paper investigated the hydrogen enriched methane/air flames diluted with CO_2. The turbulent premixed flame was stabilized on a Bunsen type burner and the two dimensional instantaneous OH profile was measured by Planar Laser Induced Fluorescence (PLIF). The flame front structure characteristics were obtained by extracting the flame front from OH-PLIF images. And the turbulence-flame interaction was analyzed through the statistic parameters. The role of hydrogen addition as well as CO_2 dilution on the features of turbulent flame were revealed by those parameters. In this work, hydrogen fractions of 0, 0.2 and CO_2 dilution ratios of 0, 0.05 and 0.1 were studied. Results showed that hydrogen addition can enhance turbulent burning velocity S_T/S_L through decreasing the scale of the finer structure of the wrinkled flame front, caused by the smaller flame instability scale. In contrast, CO_2 dilution decreased turbulent burning velocity S_T/S_L due to its inactive response to turbulence perturbation and larger flame wrinkles. For all flames, the probability density function (PDF) profile of the local curvature radius R shows a bias to positive value, resulted from the flame intrinsic instability. The PDF profile of R decreases with CO_2 dilution, while the value of local curvature radius corresponding to the peak PDF is larger. This indicates that larger wrinkles structure was generated due to CO_2 dilution, which leads to the decrease in S_T/S_L as a consequence. Hydrogen addition increases the flame volume and results in more intense combustion. CO_2 dilution has a decrease effect on flame volume for both $X_{H2} = 0$ and $X_{H2} = 0.2$ while the decrease is obvious at $X_{H2} = 0.2$, $Z_{CO2} = 0.1$. In all, hydrogen enrichment improves the combustion while CO_2 can moderate combustion. Therefore, adding hydrogen and CO_2 in natural gas can be a potential method for adjusting the combustion intensity in combustion chamber during the combustor design.

* *Corresponding author.*
E-mail address: jinhuawang@mail.xjtu.edu.cn (J. Wang).

https://doi.org/10.1016/j.ijhydene.2019.12.015

Nomenclature

A_0, A_T	laminar flame area, turbulent flame area, mm^2
ADF	accumulated density function
A_{ave}	mean turbulent flame area, mm^2
<c>	mean progress variable
F_f	mass fraction of the fuel
L_M	Markstein length, mm
Le_{eff}	effective Lewis number
l_k	Kolmogorov microscale, mm
l_λ	Taylor microscale, mm
l_0	Integral sclae, mm
l_i	flame intrinsic instability scale, mm
Ma	Markstein number
PDF	probability density function
R, R_{ave}	local curvature radius, mean local curvature radius
S_L	laminar burning velocity, cm/s
S_{Lk}	local burning velocity for the stretched flame, cm/s
S_T	turbulent burning velocity, cm/s
U	mean velocity of the mixtures at the burner outlet, m/s
u'	turbulence intensity, m/s
V_f	mean flame volume, mm^3
<W>	mean fuel consumption rate, $kg/(m^3s)$
s	flame length from origin, mm
x(s),y(s)	coordinates function of *s*
t_τ	turbulence time scale
Z_{CO2}	Dilution ratio of CO_2, %
α_D	thermal diffusivity coefficient, m^2/s
α	stretch rate, 1/s
φ	equivalence ratio
θ	angle of the contour $<c \geq 0.1$
ρ_u	density of the unburned mixture, kg/m^3
δ_L, δ_T	flame thickness, flame brush thickness, mm
κ	flame curvature, mm^{-1}
σ_{ave}	Standard deviation of the mean turbulent flame area

Introduction

The combustion of natural gas (methane is the main components) blended with hydrogen in internal combustion engines, gas turbine as well as its fundamentals [1–5] has shown an increasing study trend. Hydrogen blending in natural gas can extend the stable lean burn limit and flame propagation [6]. This effect was also found liquefied petroleum gas (LPG) combustion and biogas combustion [7–9]. Hydrogen blending in natural gas can also decrease cycle-by-cycle variations in internal combustion engines [10]. However, NOx emissions is increased substantially because of the increase of combustion temperature with hydrogen enrichment [11]. Hydrogen addition combined with EGR (Exhaust Gas Recirculation) was treated as a prospective technique to achieve the stable lean combustion and lower emissions for natural gas engine [11].

There are numerous studies conducted on this research field. Zhang et al. [12] studied the chemical kinetics of the methane/hydrogen fuel with EGR. And Hu et al. [3] investigated the fundamental laminar flame characteristics. The effect of hydrogen addition combined with EGR on flame intrinsic instability has also been investigated [3]. The nonlinear effect of hydrogen enrichment on combustion and flame intrinsic instability properties of methane has been clarified in these studies. The investigation also revealed the role of chemical reaction path on flame propagation of the methane/hydrogen fuel with EGR. Besides the laminar flame, there were also a lot of researches conducted in fundamental premixed turbulent combustion on this mixed fuel, including the turbulent burning velocity and the statistical analysis of the flame front [13–15]. Due to the government regulations on the emissions, fuel-lean combustion attracted more intentions. This requires more fundamental researches. Flame in constant volume combustion chamber is a transient flame propagation process, and it is hard to derive quantitative flame front structure information. The previous study is quite general and the comprehensive quantitative flame front structure parameters were not well obtained [10]. Due to the high density and heat capacity of CO_2, a major component of EGR, the basic turbulent combustion behavior shows large difference when EGR is introduced. In the other words, the parameters may vary significantly. Moreover, the investigations on this issue in the literature may just give an overall combustion trends, while more mechanisms on combustion process and the turbulence-flame interaction are needed.

According to the classic scale model of turbulent combustion in flamelet regime, flame is perturbed by turbulence and the turbulence-flow interaction is only kinematic. This means that only the flamelet is wrinkled while the inner flame structure and flame properties is still the laminar flame. The turbulence-flame interaction can be understood by analyzing the laminar flame properties and the character of turbulence. Therefore, in the turbulent case, the instantaneous flame front structure and its parameters are essential to the learn the combustion behavior as well as the mechanism of the turbulence-flame interaction [16].

Motivated by the consideration above, we intended to investigate the roles of the hydrogen addition and EGR dilution on the characteristics of methane/air flames, by measuring the flame front structure. Turbulent flow in a wide intensity range was generated using different perforated plates installed on a Bunsen burner [17] and measured by hot-wire anemometer. The instantaneous OH radical profile of the flame during the combustion is detected using PLIF technique to identify flame front. The character of flames and the hydrogen as well as the EGR influencing behavior are analyzed via the flame front parameters.

Experimental setup and procedures

Experimental setup and methodology

The experimental setup used in this work was fully introduced in our previous research [17,18] and a brief description

is also presented here. As shown in Fig. 1, there are three modules in the experimental system: 1) fuel/air supply system including air tank, mass flow meter and pipeline; 2) the Bunsen burner which generates the turbulence and stabilize the flame; and 3) the OH-PLIF laser diagnostic facility to measure the intermediate species concentration during the combustion. The flame was generated and stabilized on a water cooled copper nozzle-type Bunsen burner. The outlet diameter is 20 mm and the burner equipped with the sintering metal and perforated plates, used to fully mix the fuel/air, rectify the flow and to generate the turbulent flow respectively. The perforated plates with different number of orifice and orifice diameters are applied to make sure the turbulence intensity range is wide enough. To ensure the safety and stability of the main flame, an 0.5 mm annulus hydrogen diffusion pilot flame was kept at all the time during the experiments. The fuel and air were premixed before entering the Burner and would be fully mixed in a second time inside the burner. The turbulent flow and the flame condition were controlled by changing the bulk velocity and adjusting the equivalence ratio.

The single-point turbulence was measured by a high frequency hot-wire anemometer (Dantec, Stramline 90 N). The probe was placed 1.0 mm downstream of the burner exit and the data was collected at multiple measurement positions to eliminate the errors. At every position, the duration of the data collection was about 5.0 s with 30 kHz. Turbulence parameters, such as integral scale l_0, Taylor's microscale l_λ, Kolmogorov microscale, l_k were calculated by Taylor hypothesis and isotropic turbulence assumption as described in our previous studies [15,19]. We plotted all the turbulent flames in the Borghi's diagram, as shown in Fig. 2. All the tested flames are located in flamelet regime, which means we can apply flamelet concept in current study.

The instantaneous OH radical profile is detected by OH-PLIF technique [20–22]. The main components of OH-PLIF system including a Nd:YAG laser (Quanta-Ray Pro-190), a pumped dye laser (Sirah PRSC-G-3000) and an ICCD camera

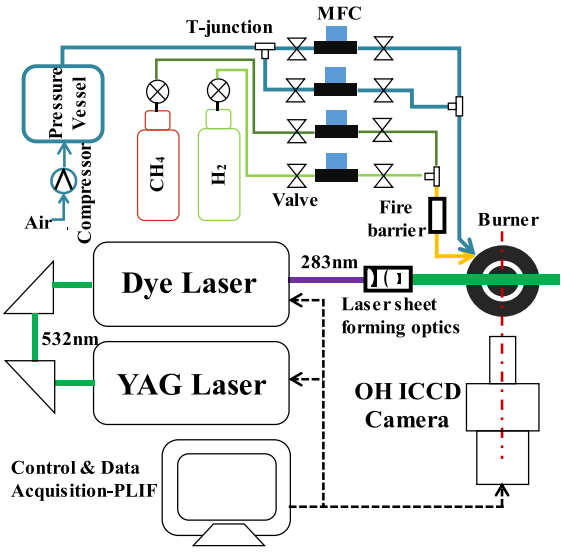

Fig. 1 – Schematic of the experimental system.

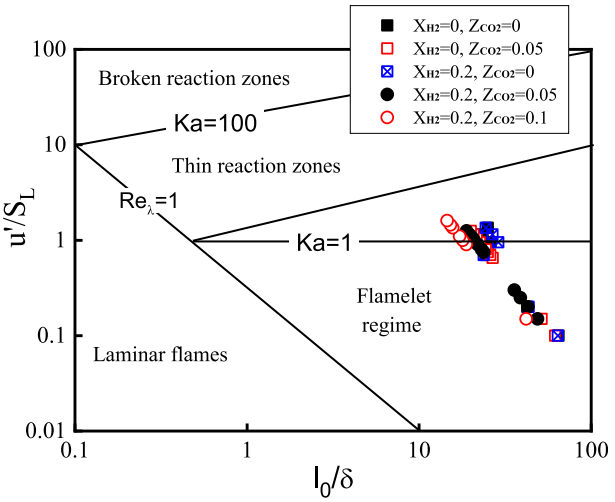

Fig. 2 – Borghi's diagram of turbulent flames revised by Peters [21].

(LaVision Image ProX) with software for signal control and data acquisition. The Nd:YAG laser source generates the raw laser with the wavelength of 532 nm at a power of 5 W. The pumped dye laser, circulating ethanol dissolved Coumarin 153, firstly doubles the frequency and then precisely adjusts the wavelength 282.769 nm, corresponding the peak of OH exciting spectrum. Finally, a laser sheet of 50×&70 mm^2 is formed through the optical elements. Fluorescence emission from excited species is optically OH bandpass filtered (LaVision VZ08-0222). The OH-PLIF images are acquired by an ICCD camera with 1280 × 1024 pixels through a UV lens (Nikon Rayfact PF 10545 MF-UV) with intensified Relay Optics (LaVision VC08-0094) at gate with of 100 ns. OH-PLIF measurement was operated at a repetition rate of 10 Hz.

Hydrogen enrichment methane flame was systematically investigated in current work. We used CO_2 to study the role of EGR on the turbulent flame since it is the main components of EGR excluding the well understood N_2. In the experiments, we mainly mixed hydrogen and CO_2 in methane, thus the ratios of those two species are defined here. The hydrogen mole fraction in the fuel is defined as the hydrogen ratio X_{H2}, expressed as $X_{H2} = Y_{H2}/(Y_{CH4}+Y_{H2})$. Analogously, the definition of CO_2 dilution ratio Z_{CO2} is the CO_2 mole fraction in the air, expressed as $Z_{CO2} = Y_{CO2}/(1\text{-}Y_{CH4}\text{-}Y_{H2})$. In above equations, Y_i represents the mole fraction species i. In this work, X_{H2} was set as 0 and 0.2 and Z_{CO2} was set as 0.05 and 0.1.

In current work, GRI-Mech 3.0 [23] was utilized as the chemical mechanism to calculated laminar flame properties, including Lewis number Le_{eff}, laminar flame speed S_L etc., with the open source code CHEMKIN-II [24]. To further clarify the flame properties, Table 1 listed all the needed parameters. Le_{eff} was originally defined as the ratio of thermal diffusivity and mass diffusivity and used as a parameter to describe diffusional-thermal instability. In this work, we calculated the effective Lewis number based on the method proposed by Dinkelacker et al. [4]. In laminar flame dynamics, the Markstein length L_M relates the local flame stretch rate and the local flame speed. Therefore, it is a representative of stretch effect and was calculated using the flame thickness δ_L and Markstein

Table 1 – Properties of mixtures in the present experiment.

X_{H2}	Z_{CO2}	φ	S_L(cm/s)	Le_{eff}	δ_L(mm)	L_M(mm)	l_i
0	0	0.9	33.98	0.9542	0.065	0.247	1.537
0	0.05	0.9	24.01	0.9390	0.093	0.339	2.018
0.2	0	0.83	33.65	0.6777	0.069	0.225	0.835
0.2	0.05	0.83	23.61	0.6635	0.099	0.307	1.016
0.2	0.1	0.83	16.28	0.6504	0.136	0.398	1.250

number Ma by the equation $L_M = \delta_L Ma$. We also provided a parameter l_i, mentioned as the flame instability scale. In the literature, it was regarded as a corresponding scale of the smallest flame wrinkles [15]. According to the non-linear flame instability formulation originated by Sivashinsky [25] and revised by Yuan et al. [26], l_i corresponds the maximum growth rate.

Image process method and geometric statistic parameters calculation

According to the flamelet concept, the sharp increase border can be regarded as the flame location. Therefore, the instantaneous flame front structure can be extracted from the profile of OH radical during the combustion, namely the images from the OH-PLIF. The methodology details were described in Refs. [20,22]. A brief summary is given here. Firstly, the 8 bits gray image was obtained from the cropped RGB image with 256 Gy intensity levels. And then the gray image was binarized by a proper threshold calculated from gray intensity histogram [27]. Last, the border of the binary image (the border of black and white region) was extracted and viewed as the location of the instantaneous flame front. Flame brush was obtained by superimposing 500 extracted flame fronts. And this can thereby determine the mean progress variable <c> of turbulent flame. For Bunsen flame, the inner and outer boundary can be identified by the <c> contours of 0.1, 0.9 respectively. In the earlier research <c> = 0.1 was also mentioned as the flame leading edge, which can be used to calculated the turbulent burning velocity S_T [15,28]. And <c> = 0.5 was regarded as the mean flame location. Once mean progress variable was determined, S_T can be obtained from <c> = 0.1 contour with the following equation,

$$s_T = U \sin\left(\theta/2\right) \tag{1}$$

where U and θ are the bulk outlet velocity and flame cone measured from the contour of <c> = 0.1.

Since the flame front is a wrinkled structure with different curvature, the local flame curvature κ, as well as the radius of curvature R, were usually employed to illustrate the flame front features. They were calculated as following,

$$\kappa = \frac{x'(s)y''(s) - y'(s)x''(s)}{(x'(s) + y'(s))^{3/2}} \tag{2}$$

$$R = K^1 \tag{3}$$

In above equation, s is the flame length from the original, and x(s) and y(s) are functions of s, representing the flame front coordinates. The first-order derivatives of the coordinate are denoted by $'$, and the second-order derivatives is denoted by $''$. It is worth to note that the step of fitting should not be too small, which will cause noise due to limited resolution, or too large, which will not capture the small scale structure. In this work, different step lengths were tried and the value of three times laminar flame thickness [29] was found as a good value in the end to calculate those two parameters. According to the definition in the literature, the structure convex to unburned gas is positive, otherwise is negative. Accumulated Density Function (ADF) can be obtained from the curvature PDF with a proper interval,

$$ADF(R) = \int_0^R PDFdR \tag{4}$$

We defined a mean flame scale of the flame front R_{ave} here. It is calculated by integrating the PDF of within a proper range as shown in Eq. (5), i.e. we use the range of −20 to 20 mm here.

$$R_{ave} = \int_0^{R^*} PDFdR + \left| \int_{-R^*}^0 PDFdR \right| \tag{5}$$

where R^* is set to be 20 mm in this study.

The instantaneous flame area, A, was defined as the instantaneous flame front occupied area by counting the pixel of the OH-PLIF binary images. The PDF distribution of instantaneous flame area A was also calculated. To further characterize the turbulent flame, global flame parameters, such as mean flame volume V_f, flame brush thickness δ_T were obtained with the same definition in Ref. [15].

Results and discussion

Instantaneous flame front and turbulent burning velocity

As discussed earlier, flamelet concept can be applied in current study, namely the flame can be viewed as a thin layer, due to the fact that most of the tested flames were in flamelet regime, as shown in Fig. 2. Fig. 3 shows the representative instantaneous flame front OH-PLIF images under different conditions. To stabilize the flame at different turbulence intensities, different perforated plates and outlet bulk inlet velocity were adjusted. The OH-PLIF images give a direct observation of the instantaneous flame front structure. We see that the flame front possesses the wrinkled structure with convex and concave structures [17]. The scale of those structures is not only affected by turbulence intensity, but there is a significant influence due to the hydrogen addition and CO_2 dilution ratio. When $X_{H2} = 0$, flame is lower and the wrinkles

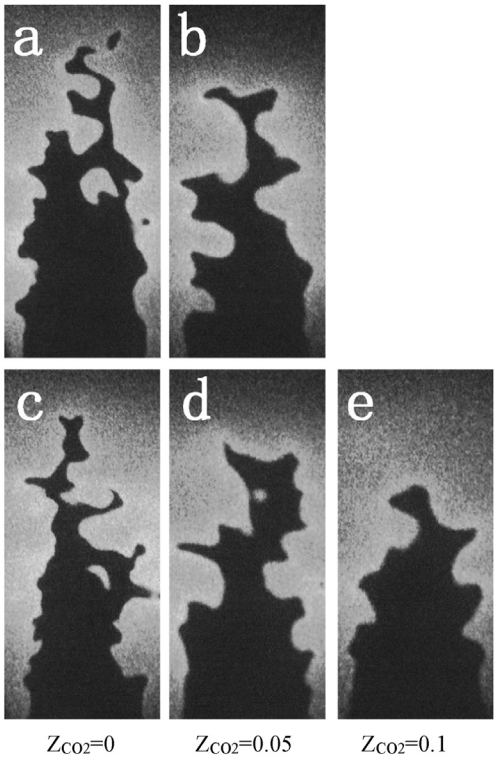

Fig. 3 – OH-PLIF images of turbulent premixed flames: (a and b) $X_{H2} = 0$, $u'/S_L \approx 1.25$; (c, d and e) $X_{H2} = 0.2$, $u'/S_L \approx 1.35$.

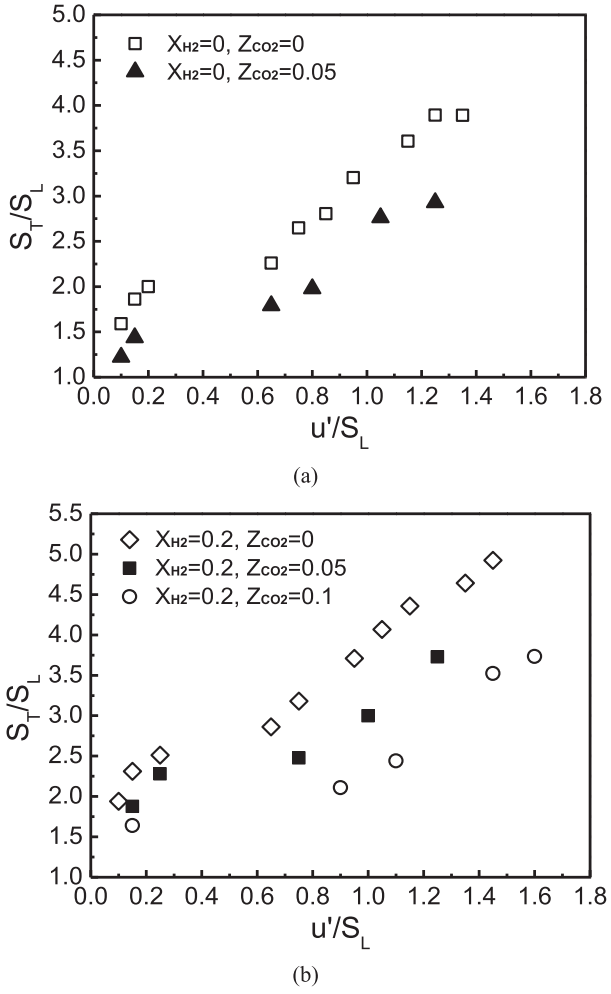

Fig. 4 – Relationship between S_T/S_L and u'/S_L for various conditions.

are less intensive when CO_2 ratio is increased. The turbulent premixed flame will be blow-off when Z_{CO2} exceeds 0.05. In the case of $X_{H2} = 0.2$, similar phenomenon is observed and the effect of CO_2 dilution is more obvious comparing to the condition of $X_{H2} = 0$. The effect of CO_2 dilution on CH_4/air flames with or without CO_2 dilution is much similar. It is very hard to extract which effect is more obvious from single image since the turbulent premixed flame is essentially random phenomenon. Subsequently, the geometrical statistical parameters are used to analyze the influence of hydrogen addition and CO_2 dilution on turbulent premixed CH_4/air flames.

Fig. 4 shows the variation of the normalized turbulent burning velocity S_T/S_L with turbulence intensity u'/S_L. Note that the data for $Z_{CO2} = 0$ at $X_{H2} = 0$ and $X_{H2} = 0.2$ is cited from the previous study of the author's group [15]. As described in Ref. [15], the normalized turbulent burning velocity S_T/S_L and turbulence intensity u'/S_L satisfies a power law relationship for the CH_4/H_2/air flames. Furthermore, the enhancement of hydrogen addition on S_T/S_L is larger under lower turbulence intensity conditions and the enhancement will be smaller at higher turbulence intensities. We can see similar results on CO_2 diluted flames that CO_2 dilution has a decreasing effect on S_T/S_L for both $X_{H2} = 0$ and $X_{H2} = 0.2$ conditions. The decreasing tendency becomes more obvious at $X_{H2} = 0.2$. This is consistent with the direct OH-PLIF image observation as shown in Fig. 3. These decreases in S_T/S_L are possibly attributed to the flame response to the local flame stretch indicated by Markstein length L_M and the flame instability scale l_i. The local flame speed relates the unstretched laminar flame speed and local flame stretch by

$$S_L - S_{Lk} = L_{M\alpha} \tag{6}$$

where α represents the stretch rate encountered by the flame. S_L is the unstretched laminar flame speed and S_{Lk} is local stretched flame speed driven by the stretch rate α. We can conclude that flame response to the stretch rate can be measured by L_M, namely, larger L_M resulting more active response. As listed in Table 1, both L_M and l_i are increased substantially with CO_2 dilution. The changes in those parameters will cause 1) smaller local flame speed, 2) larger flame wrinkles. As noted in the literature, the primary reason for the increase in the ratio of the turbulent-to-laminar flame speed is the increased flame surface area due to the wrinkled structure as [30].

$$S_T/S_L = A_T/A_0 \tag{7}$$

where A_T/A_0 are ratio of turbulent-to-laminar flame surface area. Our previous research [15] has clarified that the flame instability scale l_i has a relation with flame wrinkles. This indicates that CO_2 dilution flame has smaller the flame front area and, as a consequence, smaller S_T/S_L.

Geometric statistic flame front structure parameters

Since turbulent burning velocity is a global parameter and the analysis on the typical OH-PLIF flame image is fairly qualitative, more detailed information is needed to characterize the combustion properties. Flame curvature indicates the degree of the wrinkled structure and the radius of curvature corresponds the scale of the wrinkles. Thus those two parameters can illustrate the characteristics of the wrinkled flame front. Fig. 5 shows the probability density function (PDF) of the local curvature radius. The PDF profile shows an asymmetrical shape which has a bias to positive radius. This implies that the convex structure is more frequent, which comes from the flame properties [31]. As can be seen from the figure, when diluted with CO_2, PDF decreases for both positive and negative structure, while local curvature radius corresponding to the peak PDF distribution maintains almost the same with CO_2 dilution. The local curvature radius corresponding to the peak PDF distribution moves to smaller scale with hydrogen addition. This indicated that with CO_2 dilution, the most frequent scale maintains the same but the probability is decreased. In the case of hydrogen addition, the most frequent scale becomes smaller and the probability is increased slightly. This is attributed to the smaller Lewis number due to very fast diffusivity of hydrogen. The average curvature radius of flame front, R_{ave}, is also given in Fig. 5. R_{ave} was obtained by averaging the R value with its probability. R_{ave} decreases with hydrogen addition and increases obviously with CO_2 dilution. For further comparison with the PDF of the local radius of curvature, Fig. 6 gave the ADF profile. Similarly, ADF of positive value is higher for all tested flames. This can be further verified by the OH-PLIF image shown in Fig. 3, i.e. the flame length of convex structure is longer that concave structure, which is a general behavior of the turbulent flames. This lead to the asymmetric PDF and ADF profile. This phenomenon was also observed in Kobayashi et al. [32] for the high pressure OH-PLIF images.

The characteristics of the wrinkled flame front is critical to analyze the turbulence-flame interaction. In earlier studies, researchers usually used PDF of curvature to characterize the geometry of the wrinkled flame front, which possessed approximately symmetrical shape [33–38]. However, small curvature represents the large scale structure which is the flat segment but not the wrinkled segment, while on the contrary, what we interested is the wrinkled segment with very large curvature. The PDF of those large curvatures may be very small and is out of the range of the figure [33,39,40]. Therefore,

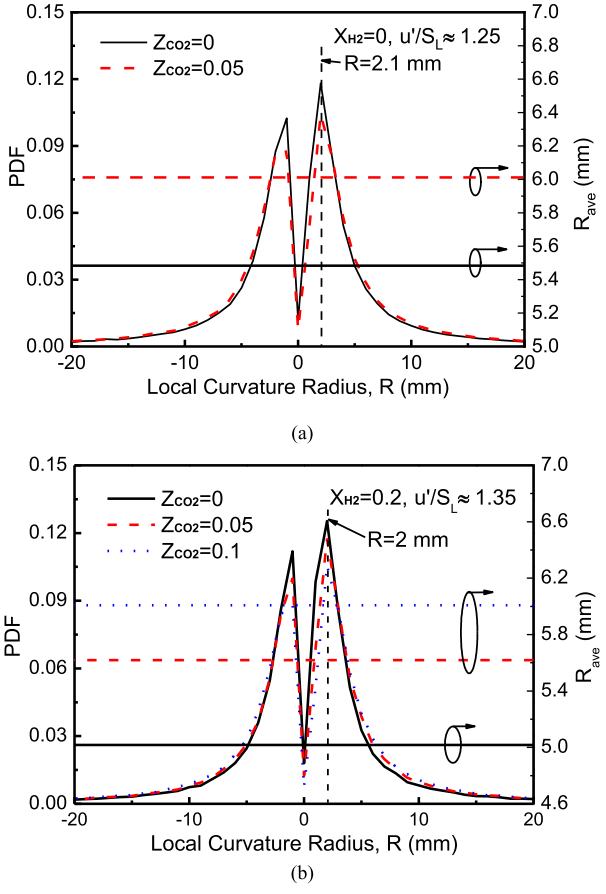

Fig. 5 – PDF distributions of the local curvature radius: (a) X_{H2} = 0; (b) X_{H2} = 0.2.

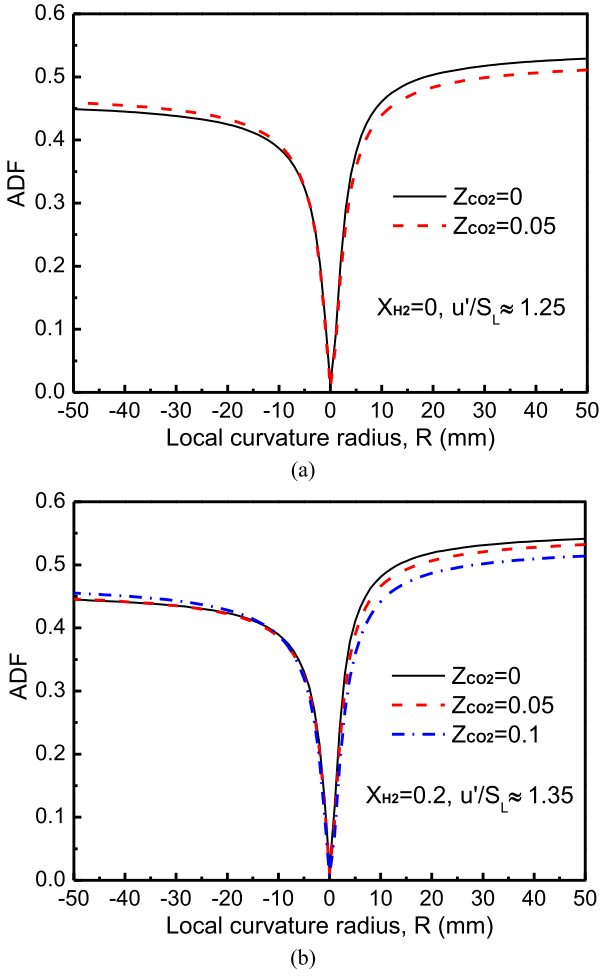

Fig. 6 – ADF distributions of the local curvature radius: (a) X_{H2} = 0; (b) X_{H2} = 0.2.

the PDF of curvature may be not adequate to illustrate to property of the turbulent flame front. For the comparison purpose, Fig. 7 showed local curvature PDF profile. The slightly positive bias distribution is also observed in the CH_4/air flames. However, the distribution is nearly symmetric with hydrogen addition and CO_2 dilution which is similar to that of previous researches [15,19]. By using the local curvature radius, the small scale structure and its distribution can be well described and a higher probability of positive structure which is convex to unburned mixtures is clearly indicated. Our previous research has revealed this positive bias distribution for turbulent premixed flames at high pressure up to 0.5 MPa [41]. In this study, the positive bias distribution is also observed at normal pressure although the bias is much weaker comparing to the high pressure flames in Ref. [41]. This indicates that the positive bias distribution should be a general characteristic for premixed turbulent flames.

Fig. 8 showed the definition of instantaneous flame area and its fluctuation. The instantaneous flame area has a significant fluctuation resulting from the feature of turbulent flame. It should be noted that the flame number has no physical meaning since the OH-PLIF image is essentially independent information with pulse laser frequency of 10 Hz. Fig. 9 plots the PDF of flame area defined in the earlier section. The mean and standard derivation of the statistical analysis of instantaneous flame area, A_{ave} and σ_A are given in Table 2. CO_2

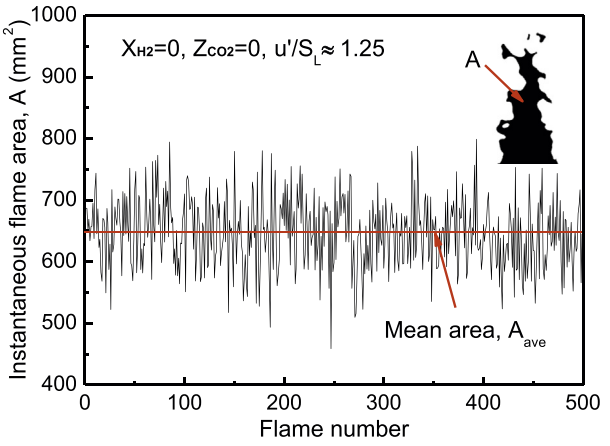

Fig. 8 – Instantaneous flame area fluctuations versus flame number.

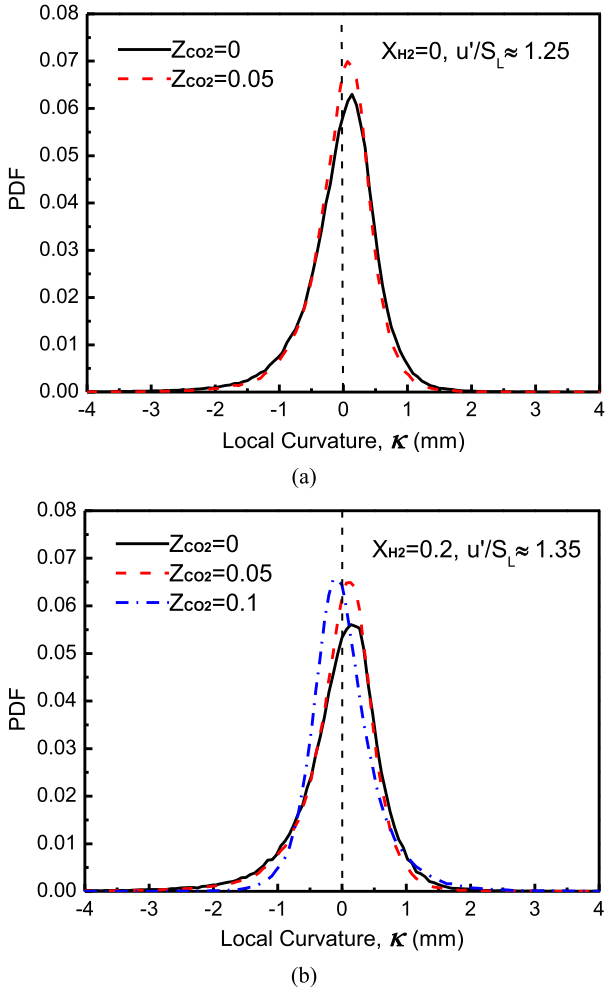

Fig. 7 – PDF distributions of the local curvature: (a) $X_{H2} = 0$; (b) $X_{H2} = 0.2$.

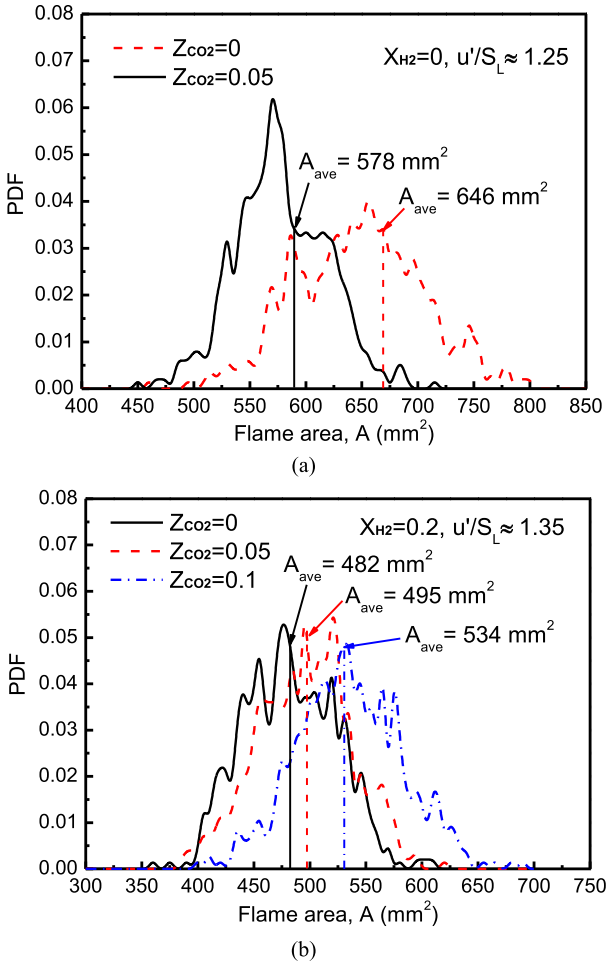

Fig. 9 – PDF distribution of the instantaneous flame area.

dilution increases the averaged flame area and this effect is more obvious at $X_{H2} = 0$. CO_2 dilution leads to more moderate heat release and less possibility of combustion oscillation [42]. In addition, the distribution profile is wider with CO_2 dilution and this effect is reflected by σ_A. This indicates that the flame has larger fluctuation with CO_2 dilution and would accelerate the flame oscillation. Those two effects must compensate each other to stabilize the flame. Further study on combustion oscillation and instability is needed.

Global parameter of the flame

In turbulent combustion model, mean fuel consumption rate of the system may relate to the mean flame volume V_f by

$$< W > = \rho_0 F_f U A / V_f \quad (8)$$

where ρ_0 is the density of the unburned mixture and F_f represents the fuel mass fraction in the mixture. Mean flame volume is a measurement of the spatial volume where chemical reaction occurs and it is a vital parameter in turbulent combustion modeling. Fig. 10 showed the variation of mean flame volume with u'/S_L. We can see from the figure that V_f is linearly increased with turbulence intensity u'/S_L. Flame volume may be affected by 1) flame height which directly influenced by outlet bulk velocity; 2) the depth of the cusps generated on the flame front resulted from the turbulence perturbation. In our experiment, for a given perforated plate, turbulence intensity is controlled by changing the outlet bulk velocity. This means higher outlet bulk velocity is needed at higher intensity, which resulted in a higher flame and deeper wrinkles, and larger mean flame volume as a consequence. When diluted with CO_2, the flame becomes shorter and inactive to the turbulence perturbation. Therefore, mean flame volume becomes smaller. V_f could be important in combustor design. In a real combustor, mean flame volume also indicates the heat release region. If it is too small, heat release is more intensive which would lead to very high temperature to damage the combustor and strong heat release also cause the combustion oscillation [43]. This would be very important for the premixed combustor design that CO_2 dilution can adjust the heat release region connected to combustion oscillation.

Another parameter which also indicates the chemical reaction occurred region layer, is flame brush thickness δ_T. δ_T is a statistical result of the instantaneous flame front location, and has universal normalizing properties which are important for the assessment of any combustion model [44,45]. It

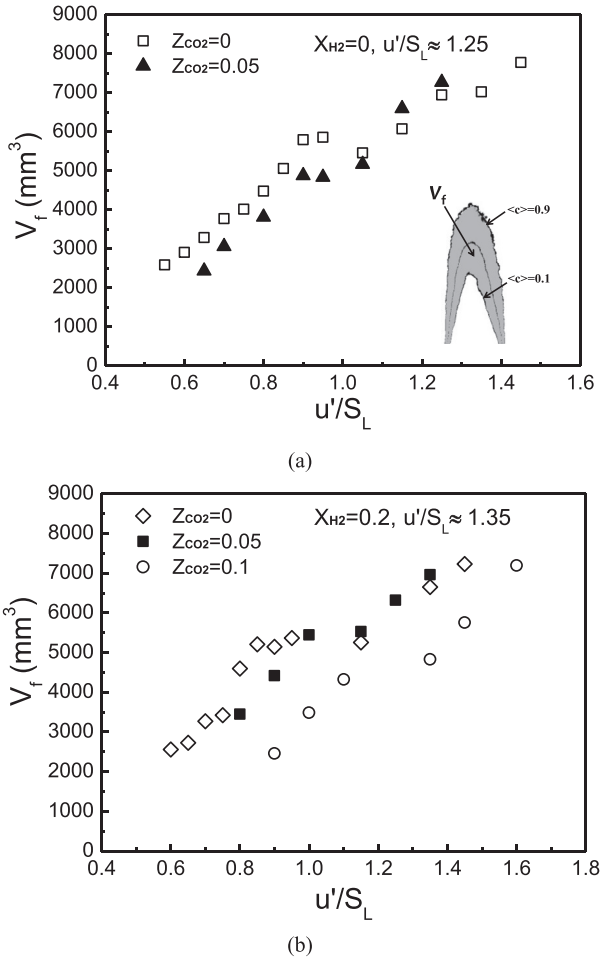

Fig. 10 – Variations of mean flame volume with u'/S_L.

connects to the turbulence intensity and integral scale, u' and l_0, as well as the turbulence time scale, t_τ [46]. Thus, the experimental measurement of δ_T is important for the assessment of numerical simulations. The definition of δ_T and relationship between δ_T versus u'/S_L are given in Fig. 11. Even though the scattering of the data, it clearly shows that δ_T increases quickly with the increase of u'/S_L and decreases with CO_2 dilution. The dilution effect is more significant in the case of $X_{H2} = 0$ than $X_{H2} = 0.2$. Similar effects on δ_T decrease is demonstrated between $X_{H2} = 0$, $Z_{CO2} = 0.05$ and $X_{H2} = 0.2$, $Z_{CO2} = 0.1$. This means that CH_4/air flame is more sensitive to CO_2 dilution.

Table 2 – Averaged and standard derivation of instantaneous flame area, A_{ave} and σ_A.

	0%H_2		20%H_2		
	$Z_{CO2} = 0$	$Z_{CO2} = 0.05$	$Z_{CO2} = 0$	$Z_{CO2} = 0.05$	$Z_{CO2} = 0.1$
A_{ave} (mm^2)	578	646	482	495	534
σ_A (mm^2)	41	56	41	42	47

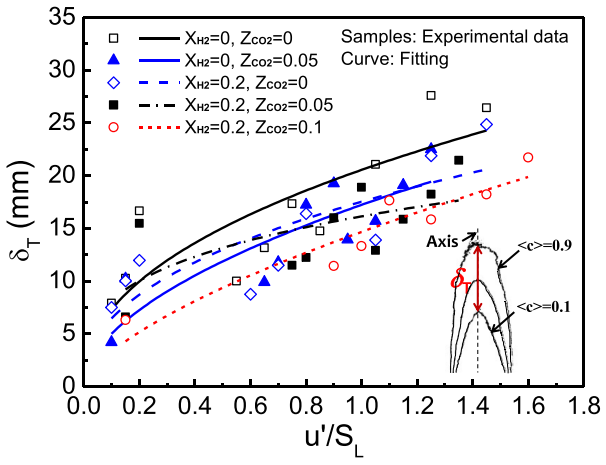

Fig. 11 – Variations of flame brush thickness with u'/S_L.

Conclusions

Turbulent flame front structure parameters of hydrogen enriched CH_4//air flames diluted with CO_2 were measured with OH-PLIF technique. The role of hydrogen addition as well as CO_2 dilution on turbulent burning velocity, flame microscopic parameters and global parameters were investigated to clarify the turbulence-flame interaction. The main conclusions are:

1. Hydrogen addition results larger turbulent burning velocity S_T/S_L due to smaller flame instability scale which can generate finer wrinkled structure. And CO_2 dilution decreased turbulent burning velocity S_T/S_L due to its inactive response to turbulence perturbation and larger flame wrinkles.
2. The probability density function profile of the local radius of curvature shows a bias to positive value, which is a general feature of the wrinkled flame front. The probability density function of local radius of curvature R for CO_2 diluted flames is lower. Moreover, the R corresponding to the peak PDF value becomes larger, meaning larger wrinkles structure was generated and leading to the decrease in S_T/S_L under CO_2 diluted conditions.
3. Hydrogen addition increases the flame volume and results in more intense combustion. CO_2 dilution has a moderate decrease on flame volume at $Z_{CO2} = 0.05$ at both $X_{H2} = 0$ and $X_{H2} = 0.2$ while the decrease is obvious at $X_{H2} = 0.2$, $Z_{CO2} = 0.1$. Hydrogen enrichment can restrain the combustion instability of natural gas and with CO_2 dilution can adjust the heat release region. Therefore, adding hydrogen and CO2 in natural gas can be a potential method for adjusting the combustion intensity in combustion chamber during the combustor design.

Acknowledgement

This study is supported by National Natural Science Foundation of China (No. 51706172, 51776164) and the China Postdoctoral Science Foundation (2017M613130, 2018T111060).

REFERENCES

[1] Wang J, Huang Z, Miao H, Wang X, Jiang D. Characteristics of direct injection combustion fuelled by natural gas–hydrogen mixtures using a constant volume vessel. Int J Hydrogen Energy 2008;33:1947–56.
[2] Akansu SO, Dulger Z, Kahraman N, Veziroglu TN. Internal combustion engines fueled by natural gas–hydrogen mixtures. Int J Hydrogen Energy 2004;29:1527–39.
[3] Hu E, Huang Z, He J, Zheng J, Miao H. Measurements of laminar burning velocities and onset of cellular instabilities of methane–hydrogen–air flames at elevated pressures and temperatures. Int J Hydrogen Energy 2009;34:5574–84.
[4] Dinkelacker F, Manickam B, Muppala SPR. Modelling and simulation of lean premixed turbulent methane/hydrogen/air flames with an effective Lewis number approach. Combust Flame 2011;158:1742–9.
[5] Wang J, Chen H, Liu B, Huang Z. Study of cycle-by-cycle variations of a spark ignition engine fueled with natural gas–hydrogen blends. Int J Hydrogen Energy 2008;33:4876–83.
[6] Tang C, Huang Z, Jin C, He J, Wang J, Wang X, et al. Laminar burning velocities and combustion characteristics of propane-hydrogen-air premixed flames. Int J Hydrogen Energy 2008;33:4906–14.
[7] Zhen HS, Leung CW, Cheung CS, Huang ZH. Combustion characteristic and heating performance of stoichiometric biogas–hydrogen–air flame. Int J Heat Mass Transf 2016;92:807–14.
[8] Zhen HS, Cheung CS, Leung CW, Choy YS. A comparison of the emission and impingement heat transfer of LPG–H2 and CH4–H2 premixed flames. Int J Hydrogen Energy 2012;37:10947–55.
[9] Zhen HS, Leung CW, Cheung CS, Huang ZH. Characterization of biogas-hydrogen premixed flames using Bunsen burner. Int J Hydrogen Energy 2014;39:13292–9.
[10] Huang ZH, Liu LX, Jiang DM, Ren Y, Liu B, Zeng K, et al. Study on cycle-by-cycle variations of combustion in a natural-gas direct-injection engine. Proc Inst Mech Eng - Part D J Automob Eng 2008;217:53–61.
[11] Hu EJ, Huang ZH, Liu B, Zheng JJ, Gu XL, Huang B. Experimental investigation on performance and emissions of a spark-ignition engine fuelled with natural gas-hydrogen blends combined with EGR. Int J Hydrogen Energy 2009;34:528–39.
[12] Zhang Y, Huang Z, Wei L, Zhang J, Law CK. Experimental and modeling study on ignition delays of lean mixtures of methane, hydrogen, oxygen, and argon at elevated pressures. Combust Flame 2012;159:918–31.
[13] Fairweather M, Ormsby MP, Sheppard CGW, Woolley R. Turbulent burning rates of methane and methane-hydrogen mixtures. Combust Flame 2009;156:780–90.
[14] Nakahara M, Shirasuna T, Hashimoto J. Experimental study on local flame properties of hydrogen added hydrocarbon premixed turbulent flames. J Therm Sci Technol 2009;4:190–201.
[15] Zhang M, Wang J, Xie Y, Wei Z, Jin W, Huang Z, et al. Measurement on instantaneous flame front structure of turbulent premixed CH4/H2/air flames. Exp Therm Fluid Sci 2014;52:288–96.
[16] Dagaut P, Egolfopoulos FN. Editorial comment. Combust Flame 2012;159:2531–2.
[17] Zhang M, Wang J, Xie Y, Jin W, Wei Z, Huang Z, et al. Flame front structure and burning velocity of turbulent premixed CH4/H2/air flames. Int J Hydrogen Energy 2013;38:11421–8.
[18] Fu J, Tang C, Jin W, Thi LD, Huang Z, Zhang Y. Study on laminar flame speed and flame structure of syngas with

varied compositions using OH-PLIF and spectrograph. Int J Hydrogen Energy 2013;38:1636–43.
[19] Zhang M, Wang J, Wu J, Wei Z, Huang Z, Kobayashi H. Flame front structure of turbulent premixed flames of syngas oxyfuel mixtures. Int J Hydrogen Energy 2014;39:5176–85.
[20] Zhang W, Wang J, Lin W, Guo S, Zhang M, Li G, et al. Measurements on flame structure of bluff body and swirl stabilized premixed flames close to blow-off. Exp Therm Fluid Sci 2019;104:15–25.
[21] Zhang W, Wang J, Guo S, Yu Q, Jin W, Zhang M, et al. Effects of integral scale on Darrieus–Landau instability in turbulent premixed flames. Flow, Turbul Combust 2019;103:225–46.
[22] Zhang M, Wang J, Chang M, Huang Z. Turbulent flame topology and the wrinkled structure characteristics of high pressure syngas flames up to 1.0 MPa. Int J Hydrogen Energy 2019;44:15973–84.
[23] Gregory P, Smith DM, Golden M, Frenklach NW, Moriarty B, Eiteneer M, et al. 1994.
[24] Kee RJ, Rupley FM, Meeks E, Miller JA. A fortran chemical kinetics package for the analysis of gas- phase chemical and plasma kinetics. Albuquerque, NM: Sandia National Laboratories; 1993.
[25] Sivashinsky GI. Instabilities, pattern formation, and turbulence in flames. Annu Rev Fluid Mech 1983;15:179–99.
[26] Yuan J, Ju Y, Law CK. On flame-front instability at elevated pressures. Proc Combust Inst 2007;31:1267–74.
[27] Wang J, Chang M, Zhang M, Li G, Chen S, Huang Z. Flame front identification and its effect on turbulent premixed flames topology at high pressure. Exp Therm Fluid Sci 2019;107:107–17.
[28] Wang J, Yu S, Zhang M, Jin W, Huang Z, Chen S, et al. Burning velocity and statistical flame front structure of turbulent premixed flames at high pressure up to 1.0 MPa. Exp Therm Fluid Sci 2015;68:196–204.
[29] Lee TW, North GL, Santavicca DA. Curvature and orientation statistics of turbulent premixed flame fronts. Combust Sci Technol 1992;84:121–32.
[30] Smallwood GJ, Gülder ÖL, Snelling DR, Deschamps BM, Gökalp I. Characterization of flame front surfaces in turbulent premixed methane/air combustion. Combust Flame 1995;101:461–70.
[31] Zhang M, Patyal A, Huang Z, Matalon M. Morphology of wrinkles along the surface of turbulent Bunsen flames – their amplification and advection due to the Darrieus–Landau instability. Proc Combust Inst 2019;37:2335–43.
[32] Kobayashi H, Nakashima T, Tamura T, Maruta K, Niioka T. Turbulence measurements and observations of turbulent premixed flames at elevated pressures up to 3.0 MPa. Combust Flame 1997;108:104–10.
[33] Lee TW, North GL, Santavicca DA. Surface properties of turbulent premixed propane/air flames at various Lewis numbers. Combust Flame 1993;93:445–56.
[34] Soika A, Dinkelacker F, Leipertz A. Pressure influence on the flame front curvature of turbulent premixed flames: comparison between experiment and theory. Combust Flame 2003;132:451–62.
[35] Lachaux T, Halter F, Chauveau C, Gökalp I, Shepherd IG. Flame front analysis of high-pressure turbulent lean premixed methane–air flames. Proc Combust Inst 2005;30:819–26.
[36] Haq MZ, Sheppard CGW, Woolley R, Greenhalgh DA, Lockett RD. Wrinkling and curvature of laminar and turbulent premixed flames. Combust Flame 2002;131:1–15.
[37] Yuen FTC, Gülder ÖL. Premixed turbulent flame front structure investigation by Rayleigh scattering in the thin reaction zone regime. Proc Combust Inst 2009;32:1747–54.
[38] Bradley D, Gaskell PH, Sedaghat A, Gu XJ. Generation of PDFS for flame curvature and for flame stretch rate in premixed turbulent combustion. Combust Flame 2003;135:503–23.
[39] Shepherd IG, Ashurst WT. Flame front geometry in premixed turbulent flames. Symposium (International) on Combustion 1992;24:485–91.
[40] Cohe C, Halter F, Chauveau C, Gokalp I, Gulder OL. Fractal characterisation of high-pressure and hydrogen-enriched CH4-air turbulent premixed flames. Proc Combust Inst 2007;31:1345–52.
[41] Wang J, Zhang M, Huang Z, Kudo T, Kobayashi H. Measurement of the instantaneous flame front structure of syngas turbulent premixed flames at high pressure. Combust Flame 2013;160:2434–41.
[42] Kobayashi H, Hagiwara H, Kaneko H, Ogami Y. Effects of CO2 dilution on turbulent premixed flames at high pressure and high temperature. Proc Combust Inst 2007;31:1451–8.
[43] Kato S, Fujimori T, Dowling AP, Kobayashi H. Effect of heat release distribution on combustion oscillation. Proc Combust Inst 2005;30:1799–806.
[44] Zhang M, Patyal A, Wang J, Huang Z. Darrieus-Landau instability effect on the flame topology and brush thickness for premixed turbulent flames. Appl Therm Eng 2019;158:113603.
[45] Lipatnikov AN, Chomiak J. Turbulent flame speed and thickness: phenomenology, evaluation, and application in multi-dimensional simulations. Prog Energy Combust Sci 2002;28:1–74.
[46] Driscoll JF. Turbulent premixed combustion: flamelet structure and its effect on turbulent burning velocities. Prog Energy Combust Sci 2008;34:91–134.